Effects of Vane Sweep on Fan-Wake/Outlet-Guide-Vane Interaction Broadband Noise

Hongbin Ju*
GE Global Research Center, One Research Circle, Niskayuna, NY. 12309

A method is developed for predicting broadband noise due to the fan-wake interacting with the downstream swept outlet-guide-vanes in turbofan jet engines. It is validated against the NASA Source Diagnostic Test data. Sweep effects on the source, on the response and on the unsteady lift coupling with the duct modes are discussed. The mechanisms of broadband noise reduction due to vane sweep are studied, and a simple model to account for sweep effects is proposed accordingly.

Keywords: Turbofan engine noise, Fan broadband noise, Aeroacoustics.

I. Introduction

The interaction of fan wakes with downstream Outlet-Guide-Vanes (OGV) is the major source of tones and broadband noise (BBN) in high bypass-ratio turbofan engines. Velocity deficit in fan wakes is the source of tone noise. Turbulence in the wakes is the source of broadband noise.

One technique to reduce tone noise is to sweep the OGV leading edges in the flow direction as shown in Fig. 1. The mechanisms of tone noise reduction in a subsonic flow were examined by Glegg [1]. The dominant effect is the phase variation of the gust introduced by the sweep. Usually the spanwise wavenumber k_3 of the velocity deficit in a fan wake is small. When the fan wake hits the swept OGV, k_3 increases and the effective frequency reduces, resulting efficient source cancellation and attenuation of acoustic waves. Secondary effects include the reduced effective inflow velocity, the introduction of the spanwise mean flow, and the reduced inter-blade phase angle (IBPA). Effects of the blade sweep on supersonic propeller noise were discussed by Parry [2].

Tone noise reduction due to vane sweep was verified numerically in [3] and experimentally in the NASA Source Diagnostic Test (SDT) [4]. BBN benefit is also shown in the SDT data. However, sweep effects on BBN have not been studied as thoroughly as for tone noise. The mechanisms for BBN noise reduction are expected to be different from for tones since vorticity waves in a turbulent flow have no dominant directions. k_3 no longer monotonically increases with the sweep angle.

The objectives of this paper are to develop a reduced order model for predicting BBN from fan-wake / swept OGV interaction, examine the sweep effects and mechanisms of noise reduction, and propose a model to account for these effects. The reduced order model is useful for preliminary designs. It is based on the semi-analytical method for oblique gust/cascade interaction in [5], and the broadband model for radial OGV in [6]. The NASA SDT data reported in [4] for low noise OGV is used to validate the method.

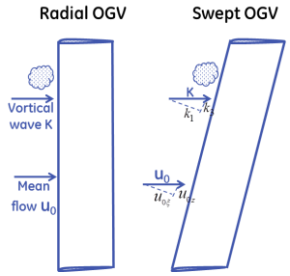

Figure 1. Radial and swept OGVs.

*Aerodynamics and Acoustics Laboratory, juh@ge.com, AIAA Senior Member

II. Broadband Model for Swept OGV in Annular Duct

The derivations of the sweep geometry and the sound power spectrum density (PSD) will be given in a separate paper. The ensemble average of PSD from cut-on modes in the annular duct is:

$$\left\langle \hat{W} \right\rangle = \sum_m \sum_n \left\langle \hat{W}_{mn} \right\rangle . \tag{1}$$

m and n are the spinning and radial mode numbers respectively. The sound power for mode (m,n) is

$$\left\langle \hat{W}_{mn}^{\pm} \right\rangle = \pm \frac{Bk_d (1-M_d^2)^2}{4\rho_d a_d \Gamma_{mn} \kappa_{mn} (k_d \mp M_d \kappa_{mn})^2} \text{Real}\left\{ \int_{R_i}^{R_o} \frac{u_0(r)\rho_0^2(r)}{S_c \cos\theta_c} E_{mn}^{\pm *}(r) \int_{-\infty}^{\infty} \left| \hat{h}_{mn}^{\pm}(K_1, K_{2m}, k_3 \mid r) \right|^2 \right.$$
$$\left. \cdot \left[\sum_{j=-\infty}^{\infty} \Phi_{ww}(K_1, K_{2m} + \frac{2\pi j}{S_c \cos\theta_c}, k_3) \right] \int_{L_1}^{L_2} E_{mn}^{\pm}(r+\Delta r) e^{i[\Theta_{mn}^{\pm}(r+\Delta r) - \Theta_{mn}^{\pm}(r)]} e^{ik_3(l_r - l'_r)/\cos\psi_s} d\Delta r dk_3 dr \right\}, \tag{2}$$

$L_1 = \max(-L_r, R_i - r)$, $L_2 = \min(L_r, R_o - r)$, L_r : spanwise turbulence length scale,

R_i, R_o : inner/outer duct radius,

$K_{2m} = \frac{2\pi m}{BS_c \cos\theta_c} - K_1 \tan\theta_c$, B: vane count, S_c : pitch, θ_c : stagger angle,

$E_{mn}^{\pm}(r) = (\alpha_{mn}^{\pm} n_x + \frac{m}{r} n_\phi)\Psi_m(\mu_{mn} r) - i\mu_{mn} \Psi'_m(\mu_{mn} r) n_r$, $\Psi_m(\mu_{mn} r)$: eigenfunction,

$$\hat{h}_{mn}^{\pm}(k_1, k_2, k_3 \mid r) = \int_0^{C_r} e^{-ix_f(\alpha_{mn}^{\pm} \cos\theta + m\sin\theta/r - k_3 \sin\psi_s)} R(\xi(x_f, r), k_1, k_2, k_3 \mid r) dx_f . \tag{3}$$

$R(\xi(x_f, r), k_1, k_2, k_3 \mid r)$ is calculated using the 2-D equivalence method in [5].

III. NASA Source Diagnostic Test (SDT) Data Analysis

The detail of the NASA SDT campaign is reported in [4]. Two rotors (R4 and M4) and three OGVs were tested. The baseline OGV has 54 radial vanes. The low vane count (LVC) OGV is also radial but with only 26 vanes. The solidity is kept constant, or the chord length is increased, to maintain the aero performance when reducing the vane count. Sweep is added to the LVC OGV to form the 3rd OGV in the test. Its leading edges are swept by 30° in the downstream flow direction, intended to reduce interaction tones. It is called the low noise (LN) OGV. The aero performance of the LN OGV is lower than the other two OGVs due to higher loading and velocity. The differences of the aero performance are small among the three OGVs near the peak efficiency. They become larger when the operation conditions are away from the peak efficiency.

The process to extract interaction BBN from the stage (rotor+stator) total noise and the fan self-noise was described in [6]. It turns out that the only data valid for the sweep study is at the approach condition. Fan self-noise is higher than the stage total noise in other operation conditions. The data for R4 rotor, the LVC OGV, and the LN OGV at the approach condition will be used in our analysis.

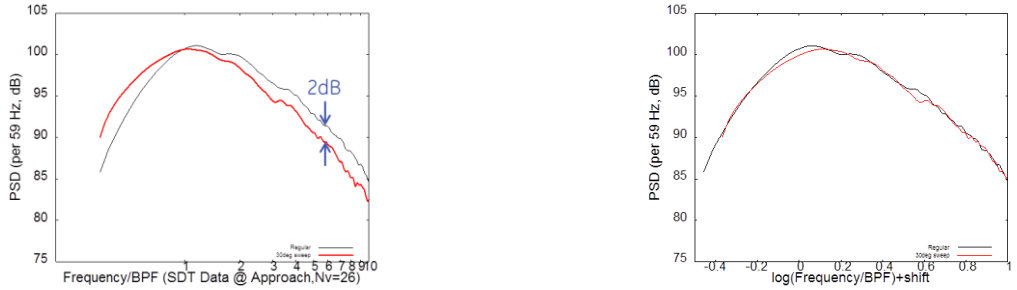

(a)Without frequency scaling **(b)With frequency scaling**

Figure 2. PSD of exhaust fan-OGV interaction broadband noise. NASA SDT data at approach. Black line: LVC radial OGV, red line: LN swept OGV.

Figure 2(a) depicts the PSD in the exhaust duct of the LN OGV compared with that of the LVC OGV. It is louder at low frequency and quieter at high frequency. The overall power level (OAPWL) is 122dB for the radial OGV, and 121dB for the swept OGV. 1dB noise reduction is achieved with the sweep. Examining the spectra in

Fig.2(a), one may find that their shapes are similar with just a shift in the log scale plot. In the linear scale, the spectrum $\hat{W}'(f')$ for the swept OGV can be obtained by scaling the frequency in the spectrum $\hat{W}(f)$ for the radial OGV:

$$\hat{W}'(f') = W(f), \quad f' = 10^{-0.09} f = 0.813 f . \tag{4}$$

With this frequency scaling, the two spectra collapse in Fig. 2(b).

IV. Validation

The proposed prediction method Eq.(1) is validated against the SDT data. Figure 3(a) shows the predicted PSD at the approach condition. The noise benefit at high frequency is about 1.3dB, compared with 2dB in the data, Fig. 2(a). The predicted OAPWL reduction with sweep is 1.2dB, compared with 1dB in the data. Similar trend is found in terms of the spectral shapes in the log scale plot: the spectrum for the swept OGV can be obtained by shifting the spectrum for the regular OGV to lower frequencies. With the same frequency scaling as in Eq.(4), the two predicted spectra in Fig. 3(b) also collapse.

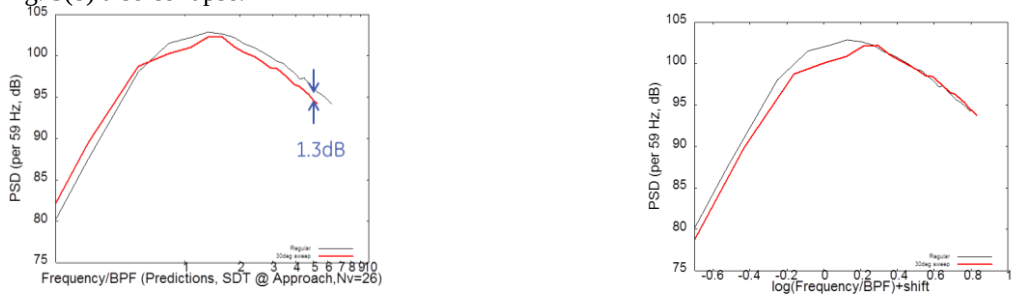

(a)Without frequency scaling **(b)With frequency scaling**

Figure 3. Predicted PSD of exhaust fan-OGV interaction broadband noise. SDT approach condition. Black line: LVC radial OGV, red line: LN swept OGV.

V. Effects of Vane Sweep

There are four major changes due to the vane sweep. The first is about the geometry. The normal chord C is reduced since the chord C_r at constant radius is maintained for aero performance. The pitch S_c and the stagger θ_c of the unwrapped linear cascade are different from the radial vane cascade. Secondly, the mean/turbulent flow is changed. Mach number increases near the tip due to the modification of the flow-path for loss control. The normal velocity to the cascade is smaller. TKE decays and the turbulence length scale increases as the flowpath to the swept OGV is longer. Thirdly, the swept OGV responds to the gusts differently. Although the reduced frequency is unchanged, the spanwise mean flow is introduced and the phase gradient of the gust varies with sweep. The last change is on the propagation. Duct modes are considered unchanged, but their coupling with the unsteady lift is different.

These changes are highlighted in Fig. 4 for the PSD formula Eqs.(2) and (3). We will discuss each of them individually. The approach of the study is to replace the parameters in each term by their counterparts in the radial OGV configuration and examine the difference of PSD. This approach is valid only when the interactions between different effects are small.

$$\left\langle \hat{W}_{mn}^{\pm} \right\rangle = \pm \frac{Bk_d (1-M_d^2)^2}{4\rho_d a_d \Gamma_{mn} \kappa_{mn} (k_d \mp M_d \kappa_{mn})^2} \int_{R_i}^{R_o} \frac{u_0 \rho_0^2}{S_c \cos\theta_c} E_{mn}^{\pm *}(r) \quad \text{(1-1)}$$

$$\cdot \int_{-\infty}^{\infty} \left| \hat{h}_{mn}^{\pm}(K_1, K_{2m}, k_3 \mid r) \right|^2 \left[\sum_{j=-\infty}^{\infty} \Phi_{ww}\left(K_1, K_{2m} + \frac{2\pi j}{S_c \cos\theta_c}, k_3\right) \right] \quad \text{(1-2)}$$

$$\cdot \int_{L_1}^{L_2} E_{mn}^{\pm}(r + \Delta r) e^{\overbrace{-i(l_S \sin\theta + l_l \cos\theta) m (1/r - 1/(r+\Delta r))}^{(3)}} e^{\overbrace{ik_3 (l_r - l'_r)/\cos\psi_s}^{(2)}} d\Delta r dk_3 dr$$

$$\hat{h}_{mn}^{\pm}(k_1, k_2, k_3 \mid r) = \int_0^{C_r} e^{-ix_f (\alpha_{mn}^{\pm} \cos\theta + m \sin\theta / r - \overbrace{k_3 \sin\psi_s}^{(4)})} \overbrace{R(\xi(x_f, r), k_1, k_2, k_3)}^{(5)} dx_f$$

Figure 4. Terms/parameters affected by sweep are highlighted in the PSD formula Eqs.(2) and (3).

To separate the effect of the mean/turbulence flow from the others, the same mean flow and turbulence statistics (TKE & length scale) are applied for both the radial and the swept OGVs. The PSD at the approach condition is shown in Fig. 5, compared with Fig.3 (a).

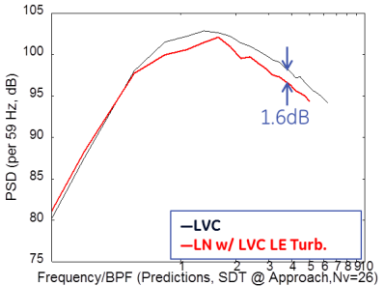

Figure 5. PSD predictions of exhaust broadband noise at the SDT approach condition. The same mean flow & turbulence statistics are applied for the radial OGV (black line) and the swept OGV (red line).

A. Effects on Source (Vorticity Waves) and Propagation (Duct Modes Coupling)

The pitch and the stagger angle are changed after sweep. However, since

$$S_c \cos\theta_c = S\cos\theta,$$

the sweep has no effect on terms (1-1) and (1-2) in Fig. 4.

Term (2) in Fig. 4 represents the spanwise phase variation as shown in Fig. 6(a). With sweep, the span is longer, giving more source cancellation and noise benefit at high frequency. With $\psi_s = 30^0$ in term (2) replaced by $\psi_s = 0$, the PSD in Fig. 6(b) changes from the blue line to the red line, indicating extra 0.67dB noise benefit due to the longer span. Assuming the noise reduction due to the source cancellation is proportional to the span, the extra benefit from the swept OGV is

$$10\log(\cos\psi_s), \text{ in dB.} \quad (5)$$

It is -0.62dB for 30^0 sweep, which is consistent with 0.67dB in the prediction shown in Fig. 6(b).

To further test the linearity of noise reduction (dB) with the span, we replace the whole term (2) in Fig. 4 by 1, i.e., totally omitting the phase variation and the source cancellation in the whole span of the swept OGV. The result in Fig. 6(b) shows significant noise increase. Since the noise benefit of the source cancellation is about 0.62dB per $6.45"\cdot\cos 30^0 \sim 0.86"$, the estimated total noise benefit for the full span 6.45" of the swept OGV is 4.6dB, not too far from 3.2dB in the prediction shown in Fig. 6(b).

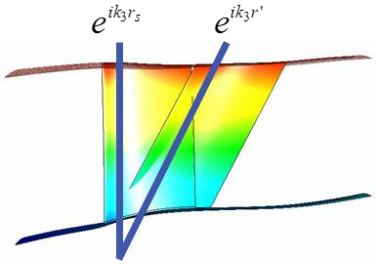

(a) Spanwise phase variation

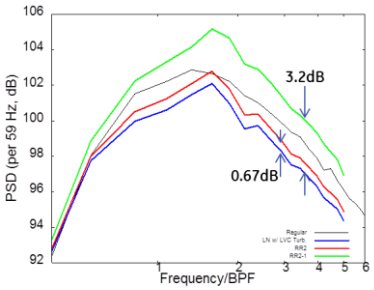

(b) PSD with different spanwise phase variations. Black line: radial OGV, blue: swept OGV, red $\psi_s = 0$ in term (2) in Fig. 4, green: term (2) replaced by 1 in Fig. 4.

Figure 6. Effect of the spanwise phase variation.

Item (3) in Fig. (4) is the effect of the phase variation with sweep in the circumferential direction, Fig 7(a). Its effect on sound power is very small as shown in Fig. 7(b). Item (4) represents the effect of the spanwise phase difference between the two TE points shown in Fig. 8(a). Its effect on sound power is also small, Fig. 8(b).

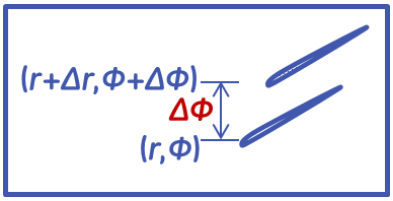

(a) Circumferential phase variation due to sweep

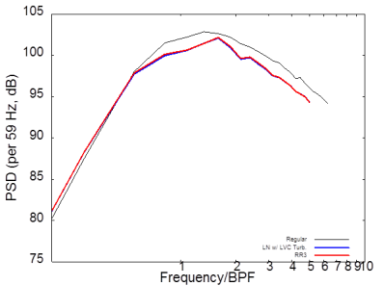

(b) PSD of exhaust broadband noise at approach. Black line: radial OGV, blue line: swept OGV, red line: item 3 in Fig. 4 replaced by 1.

Figure 7. Effect of circumferential phase variation due to sweep.

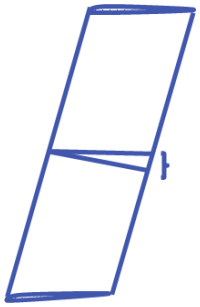

(a) Spanwise phase difference between the two TE points.

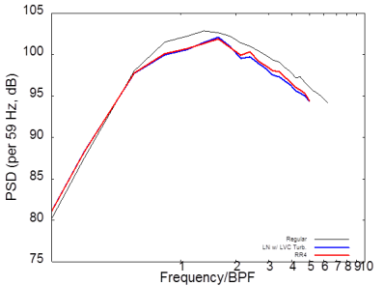

(b) PSD of exhaust broadband noise at approach. Black line: radial OGV, blue line: swept OGV, red line: item 4 in Fig. 4 replaced by 0.

Figure 8. Effect of spanwise phase difference at the trailing edges.

B. Effects on Gust/Cascade Interaction

The 2-D equivalence method [5] is employed to calculate the unsteady lift $R(\xi(x_f,r),k_1,k_2,k_3\,|\,r)$, item (5) in Fig. 4, on blades subject to oblique gusts. The effects of the five 2-D equivalent parameters are to be examined separately. The first is the Mach number

$$\overline{M} = M_\xi\sqrt{1-(\gamma k_3/\omega_e)^2}\ ,\ \gamma=\sqrt{1-M_\xi^2}\ ,\ \omega_e=\omega-k_3u_{0z}\ .$$

Fig. 9 compares the two spectra for M_ξ and for M_ξ replaced by M. They collapse when the frequency is scaled with the Mach number. That means the effect of M is simply to scale the frequency. The scaling factor is the same as in the equal turbulence energy analysis, which will be discussed later.

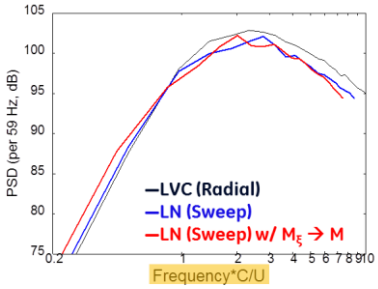

Figure 9. PSD of exhaust broadband noise at approach. Mach number effect on response. Black line: radial OGV, blue line: swept OGV, red line: M_ξ replaced by M.

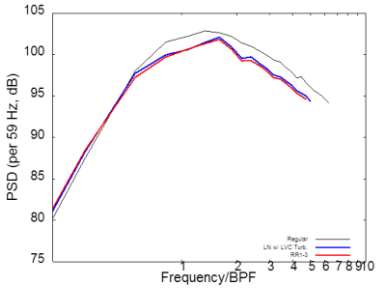

Figure 10. PSD of exhaust broadband noise at approach. Effect of stagger angle and solidity on response. Black line: radial OGV, blue line: swept OGV, red line: θ_c and S_c replaced by θ and S.

The second parameter is the 2-D equivalent IBPA:

$$\overline{\beta}_s\overline{S} = 2\pi m/B + (S_c/C)\sin\theta_c[(\bar{\gamma}/\gamma)^2-1]\lambda_e\ .$$

Since

$$(S_c/C)\sin\theta_c = (S/C_r)\sin\theta\ ,$$

the sweep has no effect on the response through IBPA.

The third and the fourth parameters are the stagger angle and the inverse solidity respectively:

$$\bar{\theta} = \tan^{-1}((\tan\theta_c)\bar{\gamma}/\gamma),\ \bar{S}/C = (S_c/C)\sqrt{\sin^2\theta_c + \cos^2\theta_c(\gamma/\bar{\gamma})^2}\ .$$

where $\bar{\gamma} = \sqrt{1-\bar{M}^2}$. If they are replaced by θ and S , the noise penalty shown in Fig. 10 is negligible.

The last parameter is the reduced frequency $\bar{\lambda} = (\bar{\gamma}/\gamma)^2\lambda_e$, with effective reduced frequency $\lambda_e = \lambda - k_3 u_{0z}/u_{0\xi}$. Since

$$\lambda = \omega C/u_{0\xi} = \omega C_r/u_0\ ,$$

the effect of the sweep is to introduce spanwise mean flow u_{0z} . When $u_{0z} = 0$ is set in λ_e , PSD shown in Fig. 11 changes very little. The reason is that gusts with k_3 =0 make the most contribution to the interaction BBN.

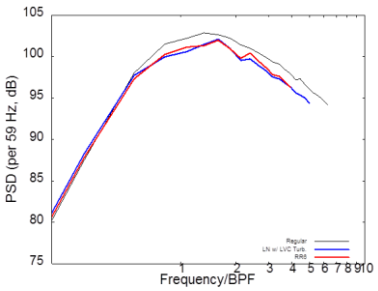

Figure 11. PSD of exhaust broadband noise at approach. Effect of spanwise mean flow on reduced frequency in response. Black line: radial OGV, blue line: swept OGV, red line: $u_{0z} = 0$ in λ_e .

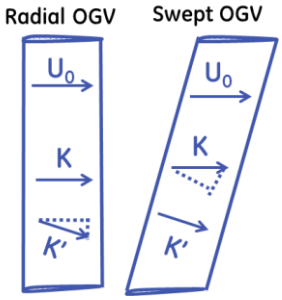

Figure 12. OGV subject to two vorticity waves.

C. Noise Penalty from Two Vorticity Waves

It is shown in Fig. 6 that the source cancellation is important for BBN even for a radial OGV. However, the BBN reduction is not due to the introduction of k_3 from vane sweep. This is the major difference between BBN and tone noise.

Let's examine two vorticity wave vectors $\vec{K}$ and $\vec{K}'$ in Fig. 12 with the same magnitude $|\vec{K}| = |\vec{K}'|$. They are normal to the radial OGV LE and the swept OGV LE respectively. For the $\vec{K}$ wave, k_3 increases with the sweep, which supposedly gives noise benefit. However, for the $\vec{K}'$ wave, k_3 reduces with sweep, causing noise penalty. The combined effect from the two waves is determined by how the benefit and the penalty compete, which can be assessed from the vorticity wave strength and the cascade response.

The strength of a vorticity wave with (k_1, k_2, k_3) in an isotropic turbulence flow is determined by the Liepmann spectrum

$$\Phi_{ww}(k_1,k_2,k_3) = \frac{2\overline{w^2}\Lambda^3}{\pi^2}\frac{(\Lambda k_1)^2 + (\Lambda k_3)^2}{[1+(\Lambda k_1)^2 + (\Lambda k_2)^2 + (\Lambda k_3)^2]^3}\ . \tag{6}$$

Λ is the turbulence integration length scale. The two waves have the same turbulence energy. However, for the vorticity wave/single airfoil interaction, the total turbulence energy generating sound is the integration of Eq.(6) over k_2 :

$$\Phi_{ww}(k_1,k_3) = \int_{-\infty}^{\infty}\Phi_{ww}(k_1,k_2,k_3)dk_2 = \frac{\overline{w^2}\Lambda^2}{4\pi}\frac{1+4(\Lambda k_1)^2 + (\Lambda k_3)^2}{[1+(\Lambda k_1)^2 + (\Lambda k_3)^2]^{2.5}}\ . \tag{7}$$

For the $\vec{K}$ wave interacting with the radial OGV,

$$\Phi_{K,ww}(k_1 = K, k_3 = 0) = \frac{\overline{w^2}\Lambda^2}{4\pi}\frac{1+4(\Lambda K)^2}{[1+(\Lambda K)^2]^{2.5}}\ . \tag{8}$$

For the $\vec{K}$ wave interacting with the swept OGV,

$$\Phi'_{K,ww}(k_1 = K\cos\psi_s, k_3 = K\sin\psi_s) = \frac{\overline{w^2}\Lambda^2}{4\pi}\frac{1+(1+3\cos^2\psi_s)(\Lambda K)^2}{[1+(\Lambda K)^2]^{2.5}}\ .$$

One can show that

$$\Phi_{K,ww} - \Phi'_{K,ww} = \frac{\overline{w^2}\Lambda^2}{4\pi}\frac{3(1-\cos^2\psi_s)(\Lambda K)^2}{[1+(\Lambda K)^2]^{2.5}} \geq 0 .$$

Similarly for the $\vec{K}'$ wave,

$$\Phi_{K',ww}(k_1 = K\cos\psi_s, k_3 = -K\sin\psi_s) = \frac{\overline{w^2}\Lambda^2}{4\pi}\frac{1+(1+3\cos^2\psi_s)(\Lambda K)^2}{[1+(\Lambda K)^2]^{2.5}},$$

$$\Phi'_{K',ww}(k_1 = K, k_3 = 0) = \frac{\overline{w^2}\Lambda^2}{4\pi}\frac{1+4(\Lambda K)^2}{[1+(\Lambda K)^2]^{2.5}}, \tag{9}$$

$$\Phi_{K',ww} - \Phi'_{K',ww} = \frac{\overline{w^2}\Lambda^2}{4\pi}\frac{3(\cos^2\psi_s - 1)(\Lambda K)^2}{[1+(\Lambda K)^2]^{2.5}} \leq 0 .$$

As the sweep angle increases, the noise-generating energy of the $\vec{K}$ wave reduces; the noise-generating energy of the $\vec{K}'$ wave energy increases.

The sound frequency from the $\vec{K}'$ wave/cascade interaction is $\omega' = -Ku_0\cos\psi_s$, which is smaller than that from the $\vec{K}$ wave/cascade interaction $\omega = -Ku_0$. In the first order, the $\vec{K}'$ wave/cascade response is stronger than the $\vec{K}$ wave. Since both the source and the response are stronger for the $\vec{K}'$ wave, the combined effect of sweep from these two waves is noise penalty. The noise reduction mechanism for tones does not apply to BBN.

D. Mechanisms & Modeling

It is shown in the last section that the introduction of k_3 with sweep for a 2-D wave on the radial OGV is counteracted by a 2-D wave on the swept OGV, and mostly the total noise from the two waves increase with sweep. Here we will show that the contributing vorticity waves are mainly the 2D waves in the respective OGVs, i.e. $\vec{K}$ in Fig. 12 for the radial OGV and $\vec{K}'$ for the swept OGV.

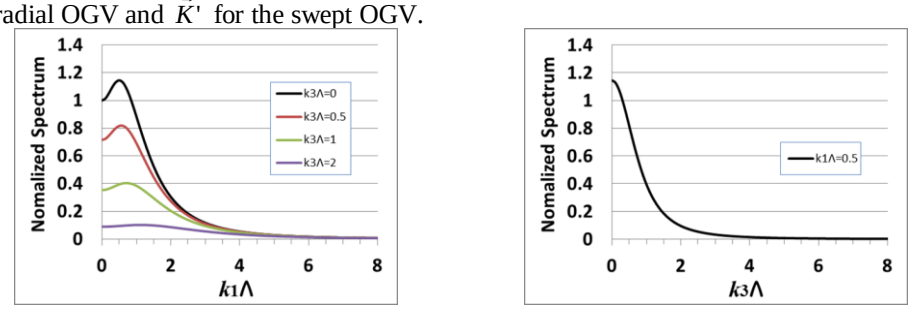

(a) (b)

Figure 13. Normalized turbulence spectrum.

Figure 13(a) illustrates the normalized spectrum:

$$\frac{\Phi_{ww}(k_1,k_3)}{\Phi_{ww}(0,0)} = \frac{1+4(\Lambda k_1)^2+(\Lambda k_3)^2}{[1+(\Lambda k_1)^2+(\Lambda k_3)^2]^{2.5}} . \tag{10}$$

The maximum turbulence energy is around $\Lambda k_1 = 0.5$, at which the maximum energy is at $\Lambda k_3 = 0$ as shown in Fig. 13(b). Therefore the vorticity waves with maximum noise-generating energy are those with $k_3 = 0$ no matter it is on the radial OGV or the swept OGV. It has been shown in [6] that if the spanwise turbulence integral length scale is small, for lower order duct modes and away from the tip or hub, noise is mainly generated by 2D gusts ($k_3 = 0$). Contributions from oblique gusts cancel each other.

Therefore, from both the source energy and the response, waves with $k_3 = 0$ are the main noise-contributing waves. On the radial OGV it is the $\vec{K}$ wave in Fig. 12. The frequency of the generated sound is $\omega = -Ku_0$. On the swept OGV, it is the $\vec{K}'$ wave with frequency $\omega' = -Ku_{0\xi} = -Ku_0\cos\psi_s$. The turbulence energies for these two waves are the same according to Eqs (8) and (9). Therefore at

$$\omega' = \omega\cos\psi_s \tag{11}$$

the main contributing vorticity waves near the swept OGV leading edges have the same energy as those near the radial OGV LEs. We have already shown that sweep has little effect on response other than the frequency scaling. Therefore, the major mechanism of BBN benefit from sweep is the frequency scaling resulted from the equal turbulence energy assumption.

The secondary effect is the source canceling and the extra benefit shown in Eq.(5) from longer span. Other changes, such as stagger/pitch, circumferential / radial phase difference, response, etc., have minimal effect on the interaction broadband noise.

From these analyses, a simple model to account for sweep effects is proposed. Assume the noise spectrum for the radial OGV is $w(\omega)$ in dB, then the noise spectrum for the swept OGV with sweep angle ψ_s is:

$$w'(\omega) = w(\omega/\cos\psi_s) + 10\log(\cos\psi_s)\text{, in dB.} \tag{11}$$

This model is applied on the test data and on the predictions in Fig. 14. In both cases the spectrum calculated from the model matches the spectrum for the swept OGV very well.

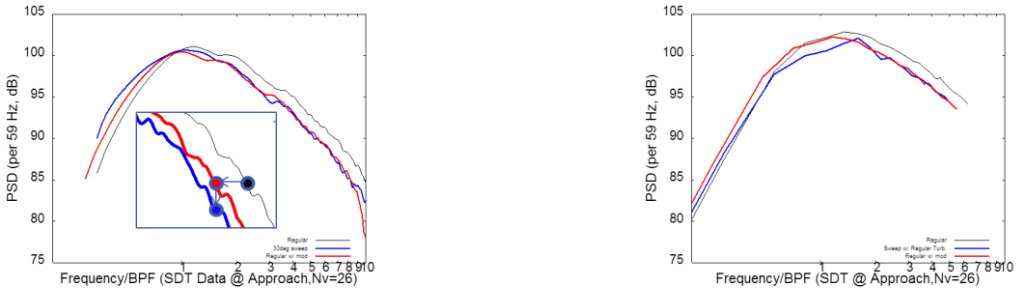

(a) Data (b) Predictions

Figure 14. PSD with sweep effects calculated using the proposed simple model Eq.(11). Black line: radial OGV, blue line: swept OGV, red line: sweep effects calculated using the model Eq.(11).

VI. Conclusions

A broadband noise prediction method was developed for fan wake/swept OGV interaction. It was validated against the NASA SDT data, and used to analyze sweep effects. It was found that the major noise-contributing vorticity waves are those normal to the OGV leading edges. The major mechanism of BBN reduction from sweep is the frequency scaling due to the equal energy of these waves. The secondary mechanism is the source cancellation over the longer span after sweep. A model was proposed to account for the two sweep effects. Predictions based on this model match with the SDT data well.

Acknowledgments

The author would like to thank his colleagues at the GE Global Research Center for their fruitful discussions: Drs. Umesh Paliath, Trevor Wood, Nikolai Pastouchenko, and Lawrence Cheung. Special thanks are due to Dr. Muni Majjigi at the GE Aviation for his permission to publish this work.

References

[1] Glegg, S. A. L., The Response of a Swept Blade Row to a Three-Dimensional Gust, Journal of Sound and Vibration, 227(1), 1999: 29~64.

[2] Parry, A.B., The Effect of Blade Sweep on the Reduction and Enhancement of Supersonic Propeller Noise, Journal of Fluid Mechanics, Vol. 293, June 1995, pp 181 – 206.

[3] Kozlov, A.V., Atassi, H.M., Logue, M.M., and Topol, D.A., Effect of Stator Vane Sweep on High Frequency Fan Noise and Comparison with Experiment, AIAA 2015-2519.

[4] Woodward R.P., Hughes, C.E., Fan Noise Source Diagnostic Test – Far-Field Acoustic Results, AIAA 2002-2427.

[5] Ju, H., Mani, R., A Semi-Analytical Method for Oblique Gust/Cascade Interaction, submitted to the AIAA Journal.

[6] Ju, H., Mani, R., Vysohlid, M., and Sharma, A., Investigation of Fan-Wake / Outlet-Guide-Vane Interaction Broadband Noise, AIAA Journal, (2015), accessed Oct. 15, 2013. doi: http://arc.aiaa.org/doi/abs/10.2514/1.J053167